

Communicating via ignorance: Increasing communication capacity via superposition of order

K. Goswami,^{1,*} Y. Cao,^{2,3} G. A. Paz-Silva,² J. Romero,^{1,†} and A. G. White¹

¹Centre for Engineered Quantum Systems, School of Mathematics and Physics, University of Queensland, QLD 4072 Australia

²Centre for Quantum Dynamics, Griffith University, Queensland 4111, Australia

³State Key Laboratory of Networking and Switching Technology,

Beijing University of Posts and Telecommunications, Beijing 100876, China

(Dated: March 30, 2020)

Classically, no information can be transmitted through a depolarising, that is a completely noisy, channel. We show that by combining a depolarising channel with another channel in an indefinite causal order—that is, when there is superposition of the order that these two channels were applied—it becomes possible to transmit significant information. We consider two limiting cases. When both channels are fully-depolarising, the ideal limit is communication of 0.049 bits; experimentally we achieve $(3.4 \pm 0.2) \times 10^{-2}$ bits. When one channel is fully-depolarising, and the other is a known unitary, the ideal limit is communication of 1 bit. We experimentally achieve 0.64 ± 0.02 bits. Our results offer intriguing possibilities for future communication strategies beyond conventional quantum Shannon theory.

Noise is ubiquitous: communication protocols aim to optimise the amount of information that can be sent through a channel with a given amount of noise. In the limit of a completely noisy channel, no information can be transmitted [1]. This is true even with a single quantum channel [2]. Surprisingly, quantum physics offers strategies to transmit information in the scenario of two noisy channels, e.g. via superposition of path [3–5], or via superposition of order [6–8]. In these strategies the superposition in a control qubit determines the superposition in path or causal order. Placing two completely noisy channels in a superposition of paths—that is in different arms of an interferometer—allows some classical information to be communicated, at least 0.16 bits when the paths are equally weighted. Placing them instead in a superposition of causal order—that is the order in which the channels are applied is indefinite—allows up to 0.049 bits to be communicated when the orders are equally weighted [6]. Here we show that using superposition of causal order, a greater communication advantage can be achieved than superposition of paths [3], ideally up to 100% of information.

We use the quantum switch, a physically realisable process that simulates the superposition of causal order, which has been implemented in several photonic experiments [9–13]. We follow the experimental setup of [11]. We analyse, and experimentally demonstrate, communication through various combinations of noisy and unitary channels in an indefinite causal order. We provide an example where perfect transmission is possible, given the freedom to choose the measurement basis of the control that determines the order. We outline the mathematical description of the channels and provide an experimental method to estimate the information-theoretic advantage quantified by the Holevo capacity, χ [14].

We depict the communication protocol in the Fig. 1. The sender maps a classical message into a quantum state $\rho_t = |\psi_t\rangle\langle\psi_t|$, which we will refer to as the target qubit. This state passes through two generalised Pauli channels \mathcal{N}_p and \mathcal{N}_q . We describe the noisy channels acting on the target qubit

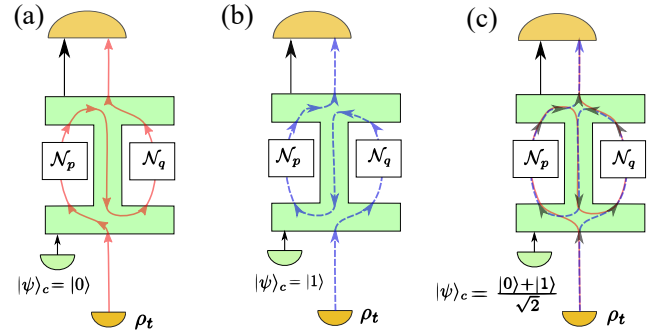


FIG. 1. Classical communication through indefinite causal order. The sender maps the classical message bit to a quantum state ρ_t —the target qubit. ρ_t passes through two noisy channels \mathcal{N}_p and \mathcal{N}_q . The order of the channels is controlled by a control qubit $|\psi_c\rangle$. (a) When the control qubit $\rho_c = |\psi_c\rangle\langle\psi_c|$ is off, i.e. $|\psi_c\rangle = |0\rangle$, the channels have a definite order $\mathcal{N}_q \circ \mathcal{N}_p$. (b) When the control qubit is on, $|\psi_c\rangle = |1\rangle$, the order is $\mathcal{N}_p \circ \mathcal{N}_q$. (c) When the control is in a superposition, $|\psi_c\rangle = (|0\rangle + |1\rangle)/\sqrt{2}$, the channels have an indefinite order.

ρ_t as

$$\mathcal{N}_p(\rho_t) = \sum_{i=0}^3 p_i \sigma_i \rho_t \sigma_i^\dagger \quad (1)$$

$$\mathcal{N}_q(\rho_t) = \sum_{i=0}^3 q_i \sigma_i \rho_t \sigma_i^\dagger, \quad (2)$$

where $\sum_i p_i = \sum_i q_i = 1$. As the equation suggests, each Pauli channel is a probabilistic mixture of all three Pauli errors via the identifications: $\sigma_1 \equiv \sigma_x$ (bit flip); $\sigma_3 \equiv \sigma_z$ (phase flip); $\sigma_2 \equiv \sigma_y$ (combination of bit flip and phase flip); and $\sigma_0 \equiv I$. The order that these two channels are applied to ρ_t is selected by a control qubit ρ_c . If the control is off, $|0\rangle_c$, then the order is $\mathcal{N}_q \circ \mathcal{N}_p$, i.e. \mathcal{N}_p is before \mathcal{N}_q . If the control is on, $|1\rangle_c$, then $\mathcal{N}_p \circ \mathcal{N}_q$. However, if the control qubit is in a superposition state, $|\psi\rangle_c = (|0\rangle + |1\rangle)_c/\sqrt{2}$, the channels \mathcal{N}_p and \mathcal{N}_q have

indefinite causal order. Specifically, given a target qubit ρ_t and a control qubit initially in the state $\rho_c = |\psi_c\rangle\langle\psi_c|$, where $|\psi_c\rangle = \sqrt{\gamma}|0\rangle + \sqrt{1-\gamma}|1\rangle$, the total output state of the switch becomes

$$\mathfrak{s}[\mathcal{N}_p, \mathcal{N}_q](\rho_c \otimes \rho_t) = \sum_{i,j} K_{ij}(\rho_c \otimes \rho_t) K_{ij}^\dagger \quad (3)$$

with

$$K_{ij} = p_i q_j (|0\rangle\langle 0| \otimes \sigma_i \sigma_j + |1\rangle\langle 1| \otimes \sigma_j \sigma_i) \quad (4)$$

In matrix representation, the overall output state becomes

$$\mathfrak{s}[\mathcal{N}_p, \mathcal{N}_q](\rho_c \otimes \rho_t) = \begin{pmatrix} A & B \\ B & \tilde{A} \end{pmatrix}, \quad (5)$$

with,

$$\begin{aligned} A &= \gamma \mathcal{N}_q \circ \mathcal{N}_p(\rho_t), \\ \tilde{A} &= (1 - \gamma) \mathcal{N}_p \circ \mathcal{N}_q(\rho_t), \\ B &= \sqrt{\gamma(1-\gamma)}(\epsilon_+(\rho_t) - \epsilon_-(\rho_t)), \end{aligned} \quad (6)$$

where (ϵ_-) ϵ_+ represents an auxiliary trace non-preserving map composed of all the operators from \mathcal{N}_p and \mathcal{N}_q that (anti-)commute. That is,

$$\epsilon_+(\rho_t) = \sum_{i=0}^3 p_i q_i \rho_t + \sum_{i=0}^3 r_{0i} \sigma_i \rho_t \sigma_i^\dagger \quad (7)$$

$$\epsilon_-(\rho_t) = r_{12} \sigma_3 \rho_t \sigma_3^\dagger + r_{23} \sigma_1 \rho_t \sigma_1^\dagger + r_{31} \sigma_2 \rho_t \sigma_2^\dagger, \quad (8)$$

with $r_{ij} = p_i q_j + p_j q_i$. Note that $\mathcal{N}_p \circ \mathcal{N}_q(\rho_t) = \epsilon_+(\rho_t) + \epsilon_-(\rho_t) = \mathcal{N}_q \circ \mathcal{N}_p(\rho_t)$, any definite order of \mathcal{N}_p and \mathcal{N}_q will have the same effect on the target qubit. To take an extreme example, if \mathcal{N}_p and \mathcal{N}_q were both completely depolarising, either of the definite orders $\mathcal{N}_p \circ \mathcal{N}_q(\rho_t)$ or $\mathcal{N}_q \circ \mathcal{N}_p(\rho_t)$ will completely scramble the target qubit.

Interestingly, the output of a quantum switch (Eqs. 5-6) implies that some information is contained in the control qubit. Depending on the outcome of a measurement in the σ_1^c basis of the control qubit, we obtain either of the conditional states $\epsilon_+(\rho_t)$ or $\epsilon_-(\rho_t)$. This means that a σ_1^c measurement allows us to estimate information encoded in the target qubit, and confirm whether there is a communication advantage when \mathcal{N}_p and \mathcal{N}_q are in an indefinite order.

In our quantum switch experiment, the control qubit is the polarisation of light. A σ_1^c measurement in this case is equivalent to a Stokes measurement $S_2(\mathfrak{s}[\mathcal{N}_p, \mathcal{N}_q])$ at the output of the quantum switch $\mathfrak{s}[\mathcal{N}_p, \mathcal{N}_q]$. As Eq. 2 suggests, the channels \mathcal{N}_p and \mathcal{N}_q can be constructed from combinations of Pauli operations $\{\sigma_i\}$ acting on the target qubit. In the supplementary material, we show how $S_2(\mathfrak{s}[\mathcal{N}_p, \mathcal{N}_q])$ can be calculated from Stokes measurements $S_2(\mathfrak{s}[\sigma_i, \sigma_j])$ at the output of a quantum switch of σ_i and σ_j , $\mathfrak{s}[\sigma_i, \sigma_j]$. This means that rather than physically implementing $\mathfrak{s}[\mathcal{N}_p, \mathcal{N}_q]$, we can simply use Stokes measurements from $\mathfrak{s}[\sigma_i, \sigma_j]$, so long as we keep

σ_i	σ_j	$\tilde{\rho}_t$	$\tilde{\rho}_c$	$S_2(\mathfrak{s}[\sigma_i, \sigma_j])^{\text{theor.}}$	$S_2(\mathfrak{s}[\sigma_i, \sigma_j])^{\text{exp.}}$
σ_0	σ_0	$ 1\rangle$	D	1	0.8547 ± 0.0006
	σ_1	$ 0\rangle$	D	1	0.8718 ± 0.0005
	σ_2	$-i 0\rangle$	D	1	0.8792 ± 0.0005
	σ_3	$- 1\rangle$	D	1	0.8823 ± 0.0005
σ_1	σ_0	$ 0\rangle$	D	1	0.8459 ± 0.0006
	σ_1	$ 1\rangle$	D	1	0.8439 ± 0.0007
	σ_2	$-i 1\rangle$	A	-1	-0.8434 ± 0.0006
	σ_3	$- 0\rangle$	A	-1	-0.8540 ± 0.0007
σ_2	σ_0	$-i 0\rangle$	D	1	0.8473 ± 0.0007
	σ_1	$i 1\rangle$	A	-1	-0.8600 ± 0.0005
	σ_2	$ 1\rangle$	D	1	0.8447 ± 0.0006
	σ_3	$i 0\rangle$	A	-1	-0.8278 ± 0.0008
σ_3	σ_0	$- 1\rangle$	D	1	0.8316 ± 0.0006
	σ_1	$ 0\rangle$	A	-1	-0.8228 ± 0.0006
	σ_2	$-i 0\rangle$	A	-1	-0.8575 ± 0.0006
	σ_3	$ 1\rangle$	D	1	0.8780 ± 0.0005

TABLE I. Data used to calculate the Holevo capacity using Eq. 9 for the different combinations of unitary operations σ_i and σ_j . $\tilde{\rho}_t$ and $\tilde{\rho}_c$ are the output target and control state respectively. $S_2(\mathfrak{s}[\sigma_i, \sigma_j])$ is the Stokes parameter obtained by measuring polarisation of the control qubit in the diagonal/anti-diagonal basis after the unitaries σ_i and σ_j . We list both the theoretically expected values, $S_2(\mathfrak{s}[\sigma_i, \sigma_j])^{\text{theor.}}$, and the experimentally measured values, $S_2(\mathfrak{s}[\sigma_i, \sigma_j])^{\text{exp.}}$, of this Stokes parameter. Error bars (1σ) were calculated by propagation of error on the individual Stokes parameter with Poissonian counting statistics.

track of the Pauli operations we perform, in effect using an additional memory. The detailed description of our quantum switch and how we implemented the operations $\{\sigma_i\}$ on the transverse spatial mode—our target qubit—can be found in the Supplementary Material.

The Stokes parameters $S_2(\mathfrak{s}[\sigma_i, \sigma_j])$ are important because we use these to obtain the output control qubit $\tilde{\rho}_c$ after tracing out the target qubit. With knowledge of $\tilde{\rho}_c$, we can then calculate the Holevo capacity $\chi(\mathfrak{s}[\mathcal{N}_p, \mathcal{N}_q])$ —a measure of the maximum amount of classical information that can be transferred through our arrangement of indefinitely ordered channels. This is given by [6]:

$$\chi(\mathfrak{s}[\mathcal{N}_p, \mathcal{N}_q]) = 1 + H(\tilde{\rho}_c) - H^{\min}(\mathfrak{s}[\mathcal{N}_p, \mathcal{N}_q]), \quad (9)$$

where $H^{\min}(\mathfrak{s}[\mathcal{N}_p, \mathcal{N}_q])$ is the minimum entropy of the two-qubit output of the quantum switch, and $H(\tilde{\rho}_c)$ is the von-Neumann entropy of the output control qubit $\tilde{\rho}_c$ (see Supplementary Material for explicit expressions in terms of $S_2(\mathfrak{s}[\sigma_i, \sigma_j])$).

In our experiment, we implemented the quantum switch with all 16 pairs of σ_i and σ_j , as shown in Table I. We measured $S_2(\mathfrak{s}[\sigma_i, \sigma_j])$, i.e. the diagonal and anti-diagonal components of the polarisation of the output light, for each pair σ_i, σ_j , with the control qubit initialised to $|\psi\rangle_c = (|0\rangle + |1\rangle)_c / \sqrt{2}$ —diagonally polarised light. We measure over 10 s; the measured rate at the control output is around 100,000 counts per second. Table I summarises the results. The first two columns are the ideal settings for the target operations on the transverse spatial mode, σ_i, σ_j , the third and fourth columns are the ideal output transformations,

$\tilde{\rho}_t, \tilde{\rho}_c$ of the target and control qubits, respectively. Fig. 2 shows the action of the transformations from column 3 on our choice of input target qubit. The last two columns are the ideal and measured values of the Stokes parameter of the control output. We minimise the uncertainty in each measurement by accumulating a large number of counts. Computer-controlled waveplates, with angular orientation uncertainty of $\pm(2.5 \times 10^{-4})^\circ$, are used to measure in the diagonal/anti-diagonal basis. Our measurements are limited by the non-ideal interferometric visibility in our switch. We calculate the average visibility from the values mentioned in Table I, which is $85 \pm 2\%$. This is due to several factors. We use inverting prisms that have relatively coarse rotation accuracy $\pm 1^\circ$ to perform the unitary operations on the spatial mode. Moreover, each optical element is not perfectly flat, introducing wavefront distortions that limit the final visibility.

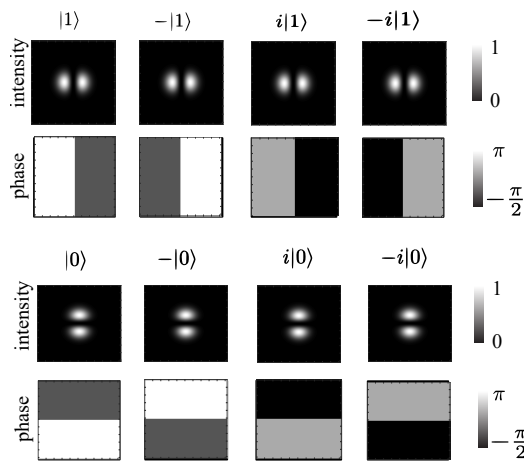


FIG. 2. Predicted spatial mode of target qubit outputs, $\tilde{\rho}_t$, after the Pauli operations $\{\sigma_i, \sigma_j\}$ (see columns 1–3 of Table I). The input target qubit ρ_t is $|1\rangle = \text{HG}_{10}$, a first-order Hermite-Gaussian mode.

Now that we can calculate the output control qubit from Table I, we can use Eq. 9 to estimate the Holevo capacity χ . We compare the experimental and predicted Holevo capacities for several combinations of channels. We first consider a quantum switch $\mathfrak{s}[\mathcal{N}, \mathcal{N}]$ of two depolarizing channels \mathcal{N} of identical strengths q , i.e. in Eq.2 we set all coefficients to $q/4$:

$$\mathcal{N} = (1 - 3q/4)\rho_t + q/4(\sigma_1\rho_t\sigma_1 + \sigma_2\rho_t\sigma_2 + \sigma_3\rho_t\sigma_3), \quad (10)$$

This scenario was theoretically studied in Ref. [6]. Experimental and predicted Holevo capacities are shown in Fig. 3, which plots the logarithm of χ against increasing q . The red circles are our measured values; the orange shaded region is the predicted Holevo capacity for visibilities of $85 \pm 2\%$; the black curve is the Holevo capacity for an ideal quantum switch. The blue curve is the ideal Holevo capacity for two depolarising channels in some definite order which—as expected—decreases monotonically with increasing depolarising strength. In the limit of two fully depolarising channels, $q=1$, $\chi=0$ bits are transmitted using definite order. In this limit there is a clear advantage in using quantum channels: ideally 4.9×10^{-2} bits can be transmitted, we measure

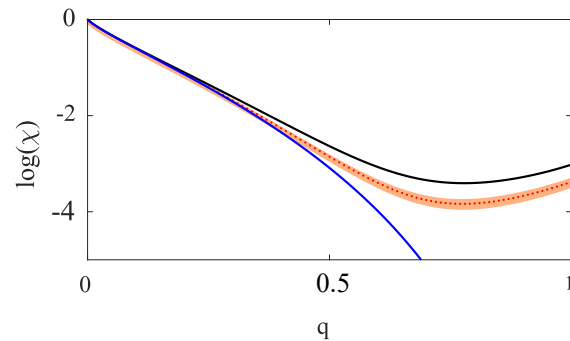


FIG. 3. Logarithm of Holevo capacity χ , of two identical depolarising channels, versus depolarising channel strength, q . The blue line is the predicted Holevo capacity for the case of definite order. The black line is the predicted Holevo capacity for the case of indefinite order. The red dots are the measured values for Holevo capacity in our quantum switch; in excellent agreement with the predicted Holevo capacity for our experimental visibilities $85 \pm 2\%$, shown by the orange shaded area. Note that the minimum measured Holevo capacity of $\chi = (2.1 \pm 0.2) \times 10^{-2}$ bits occurs at a depolarisation $q = 0.78$, and that higher capacity of $\chi = (3.4 \pm 0.2) \times 10^{-2}$ bits occurs at full depolarisation, $q = 1$.

$\chi = (3.4 \pm 0.2) \times 10^{-2}$ bits. This is a rather counterintuitive result as, individually none of the channels can transmit any information.

This nonzero Holevo capacity can be understood intuitively from the fact that the output of a quantum switch with two depolarising channels is a statistical mixture of the output of a quantum switch with different Pauli operations $\{\sigma_i\}$. Some of these Pauli operations anti-commute, hence superpositions of the order of anti-commuting Pauli operations can preserve a finite amount of information in the target qubit.

This intuition helps us understand another striking prediction, which is that above some non-zero depolarisation strength the Holevo capacity will increase. In the ideal case, we see that Holevo capacity attains a minimum value of 3.3×10^{-2} bits at $q = 0.78$ and then the capacity increases to the limit of 4.9×10^{-2} bits at $q = 1$, in stark contrast to the classical case of definite causal order which decreases monotonically to zero. Experimentally, we see this increase in information capacity from $\chi = (2.1 \pm 0.2) \times 10^{-2}$ bits at $q = 0.78$, i.e. at its worst absolute performance it is 13.5σ above the classical performance at that value of q .

We look at Eq. 9 to understand this behaviour: for low depolarisation strengths, the minimum entropy $H^{\min}(\mathfrak{s}[\mathcal{N}_p, \mathcal{N}_q])$ increases more rapidly than the von Neumann entropy $H(\tilde{\rho}_c)$. This means that for low q , the rate of depolarisation of the composite system—target and control—is faster than the rate of depolarisation of the control qubit. However, at $q \approx 0.78$, $H(\tilde{\rho}_c)$ begins to increase more rapidly than $H^{\min}(\mathfrak{s}[\mathcal{N}_p, \mathcal{N}_q])$ so the depolarisation rate of the control overtakes the depolarisation rate of the composite system, and the information revival occurs.

Consequently, as a second example we consider the quan-

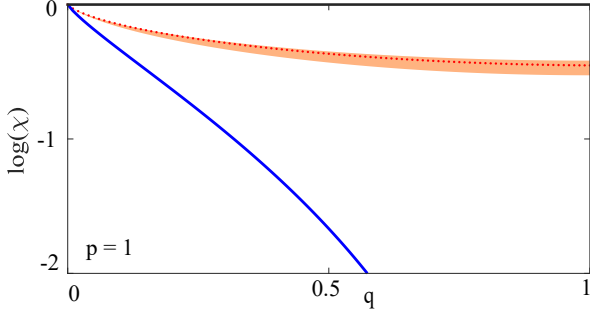


FIG. 4. Logarithm of Holevo capacity χ , where one channel is a depolarising channel of varying strength q , and the other is a σ_3 channel, the channel in Eq. (11) with $p=1$. The solid black line ($\log(\chi)=0$) is the theoretical predictions for Holevo capacity for indefinite causal order. The orange shade show the uncertainty due to non-ideal visibility in our experiment. The red dots are the experimentally measured data points and the blue line is the theoretical predictions for Holevo capacity for definite order. We show the special case for $p=1$, i.e. the dephasing channel becomes a σ_3 channel. Note that in this situation, indefinite causal order allows us to get full 1 bit information. Experimentally we measure a Holevo capacity of 0.64 ± 0.02 bits at $q=1$.

tum switch $\mathfrak{s}[\mathcal{N}, \mathcal{M}]$ composed of a depolarizing channel \mathcal{N} of strength q (Eq. 10) and a dephasing channel \mathcal{M} of strength p given by:

$$\mathcal{M} = [(1-p)\rho_t + p\sigma_3\rho_t\sigma_3]. \quad (11)$$

When $q=1$, any definite order of these two channels results in a fully depolarizing channel, regardless of the value of p , thus $\chi=0$. However, with the additional freedom to prepare and measure the control qubit, the Holevo capacity of these two channels in indefinite order, $\chi(\mathfrak{s}[\mathcal{N}, \mathcal{M}]) \equiv \chi_i$ can be non-zero and is a function of p . In fact, this combination achieves the maximum value of 1 bit when $p=1$ regardless of the depolarisation strength q , as shown in Fig. 4 (black line). We emphasise the contrast with the zero capacity of the definitely ordered channels at $q=1$, Fig. 4 (blue line).

This unit Holevo capacity can be understood by noting that when $p=1$, \mathcal{M} is a unitary channel and the conditional states become:

$$\begin{aligned} \epsilon_+(\rho_t) &= (q/4)\rho_t + (1-3q/4)\sigma_3\rho_t\sigma_3, \\ \epsilon_-(\rho_t) &= q/4(\sigma_1\rho_t\sigma_1 + \sigma_2\rho_t\sigma_2). \end{aligned} \quad (12)$$

and thus from Eq. 9 $\chi_i = 1 + H(\tilde{\rho}_c) - H_{\rho_t}^{\min}[\epsilon_+(\rho_t) \oplus \epsilon_-(\rho_t)]$, where $H(\cdot)$ is again the von Neumann entropy and the minimisation is done over all possible target states. Notice that the states that minimize the entropy of $\epsilon_+(\rho_t) \oplus \epsilon_-(\rho_t)$ are the eigenvectors of σ_3 . Take $\rho = |0\rangle\langle 0|$ as an example, $\epsilon_+(\rho_t) = (1-q/2)|0\rangle\langle 0|$, while $\epsilon_-(\rho_t)$, will be $(q/2)|1\rangle\langle 1|$ in which case, $H[\epsilon_+(\rho) \oplus \epsilon_-(\rho)] = H(q/2)$, and thus the Holevo-capacity of the quantum switch becomes 1 bit [15]. We compare our experimental and predicted χ_i in Fig. 4, red dots are experimental values and the orange shaded regions accounts

for non-ideal visibility. For full depolarisation at $q=1$, we show 0.64 ± 0.02 bits compared to the ideal case of $\chi_i=1$. Interestingly, this ideal capacity is strictly larger than the one achieved in Ref.[16] given the same channels in a path superposition. More strongly, in the Supplementary Material, we prove that these channels in a superposition of path cannot lead to unit capacity. We also compare predicted and experimental χ_i for other dephasing strengths p in the Supplementary Material.

We note that when [6] proposed communication advantage from indefinite causal order they did not claim that the advantage is unique to coherent superposition of order. Subsequently, there has been an active discussion on the origin of the communication advantage [16–18] with consensus yet to be reached. The experimental developments in the present work and [13] are further motivation to develop a well-defined resource communication theory featuring coherence.

Quantum mechanics allows indefinite causal order, which allows us to communicate up to 1 (0.049) bits of information through one (two) fully depolarising channels. This opens up interesting applications. Consider a situation where we wish to communicate through a field channel which is noisy in the target degree of freedom but unitary in the control degree of freedom, e.g. the atmosphere is noisy for spatial mode, but preserves polarisation. We can establish a lab channel that is unitary in both the control and target degrees of freedom, and place it in indefinite causal order with the field channel. The control system can be low-dimension—qubits—whereas the target degree of freedom may be of higher dimension—qudits—so this enables communication through a channel that is otherwise completely noisy for qudits. Note that the field channel must be one that is naturally a return channel—i.e. the field channel exits and reenters the lab—since it is being used in indefinite causal order. The architecture presented in this paper can be useful for imaging through turbid media where the information being communicated is the modulation of the spatial mode. Possible examples are imaging through skin or establishing a return channel to a satellite, in both cases, the midpoint of the noisy return channel is providing modulation information that would normally be entirely lost.

We can also use this idea for secret sharing, where a specific combination of channels, when connected indefinitely, can transfer information between two parties, but in a scenario of eavesdropping, any intervention will break the ‘indefiniteness’, and the message will remain scrambled.

Acknowledgements. We thank Prof Howard Wiseman for suggesting this collaboration. We also thank Prof. Giulio Chiribella for a helpful discussion. KG thanks the organisers of the Quantum Information Structure Of Spacetime, 2020 workshop where valuable insights related to this work were discussed. This work has been supported by: the Australian Research Council (ARC) by Centre of Excellence for Engineered Quantum Systems (EQUS, CE170100009), a DECRA grant (DE160100409), Advance Queensland Funding, and L’Oreal-UNESCO FWIS grant for JR; a DECRA grant (DE170100088) for GPS; YC is supported by a CSC schol-

arship; the University of Queensland by a Vice-Chancellor's Senior Research and Teaching Fellowship for AGW; and the John Templeton Foundation (the opinions expressed in this publication are those of the authors and do not necessarily reflect the views of the John Templeton Foundation). We acknowledge the traditional owners of the land on which the University of Queensland is situated, the Turrbal and Jagera people.

tum Information (Cambridge University Press, 2000).

* k.goswami@uq.edu.au

† m.romero@uq.edu.au

- [1] C. E. Shannon, *The Bell System Technical Journal* **27**, 379 (1948).
- [2] J. Preskill, arXiv: 1604.07450 (2016).
- [3] A. A. Abbott, C. Giarmatzi, F. Costa, and C. Branciard, *Phys. Rev. A* **94**, 032131 (2016).
- [4] N. Gisin, N. Linden, S. Massar, and S. Popescu, *Phys. Rev. A* **72**, 012338 (2005).
- [5] G. Chiribella and H. Kristjánsson, *Proceedings of the Royal Society A: Mathematical, Physical and Engineering Sciences* **475**, 20180903 (2019).
- [6] D. Ebler, S. Salek, and G. Chiribella, *Phys. Rev. Lett.* **120**, 120502 (2018).
- [7] S. Salek, D. Ebler, and G. Chiribella, arXiv:1809.06655 (2018).
- [8] G. Chiribella, M. Banik, S. Bhattacharya, T. Guha, M. Alimuddin, A. Roy, S. Saha, S. Agarwal, and G. Kar, arXiv:1810.10457 (2018).
- [9] L. M. Procopio, A. Moqanaki, M. Araújo, F. Costa, I. Alonso Calafell, E. G. Dowd, D. R. Hamel, L. A. Rozema, Č. Brukner, and P. Walther, *Nature Communications* **6**, 7913 (2015).
- [10] G. Rubino, L. A. Rozema, A. Feix, M. Araújo, J. M. Zeuner, L. M. Procopio, Č. Brukner, and P. Walther, *Science Advances* **3**, e1602589 (2017).
- [11] K. Goswami, C. Giarmatzi, M. Kewming, F. Costa, C. Branciard, J. Romero, and A. G. White, *Phys. Rev. Lett.* **121**, 090503 (2018).
- [12] K. Wei, N. Tischler, S.-R. Zhao, Y.-H. Li, J. M. Arrazola, Y. Liu, W. Zhang, H. Li, L. You, Z. Wang, Y.-A. Chen, B. C. Sanders, Q. Zhang, G. J. Pryde, F. Xu, and J.-W. Pan, *Phys. Rev. Lett.* **122**, 120504 (2019).
- [13] Y. Guo, X.-M. Hu, Z.-B. Hou, H. Cao, J.-M. Cui, B.-H. Liu, Y.-F. Huang, C.-F. Li, G.-C. Guo, and G. Chiribella, *Physical Review Letters* **124** (2020), 10.1103/physrevlett.124.030502.
- [14] A. Holevo, *Journal of Problems in Information Theory* **9**, 177 (1973).
- [15] This maximum advantage over definite order is also attained by having an indefinite order of one fully depolarising channel and a unitary σ_2 or σ_3 channel, when the input states are the eigenstates of σ_2 and σ_3 , respectively.
- [16] A. Abbott, J. Wechs, D. Horsman, M. Mhalla, and C. Branciard, arXiv: 1810.09826 (2018).
- [17] P. A. Guérin, G. Rubino, and C. Brukner, *Phys. Rev. A* **99**, 062317 (2019).
- [18] H. Kristjánsson, S. Salek, D. Ebler, and G. Chiribella, arXiv:1910.08197 (2019).
- [19] G. G. Stokes, *Trans. Cambridge Philos. Soc* **9**, 399 (1852).
- [20] J. Leach, J. Courtial, K. Skeldon, S. M. Barnett, S. Franke-Arnold, and M. J. Padgett, *Phys. Rev. Lett.* **92**, 013601 (2004).
- [21] M. Nielsen and I. Chuang, *Quantum Computation and Quan-*

SUPPLEMENTARY MATERIAL

Estimating the Stokes parameter of the quantum switch

With the Pauli decomposition discussed above, we now show how measurements of the control qubit, $\tilde{\rho}_c$, can be used to estimate the Holevo capacity. Since our control qubit is polarisation, we express the output control in terms of the Stokes vector (S_1, S_2, S_3) [19]:

$$\tilde{\rho}_c = \frac{1}{2} \begin{pmatrix} 1+S_1 & S_2+iS_3 \\ S_2-iS_3 & 1-S_1 \end{pmatrix}. \quad (\text{S1})$$

From Eq.5, if we measure the output control state, $\tilde{\rho}_c$ becomes,

$$\begin{aligned} \tilde{\rho}_c &= \begin{pmatrix} \text{Tr}(A) & \text{Tr}(B) \\ \text{Tr}(B) & \text{Tr}(\tilde{A}) \end{pmatrix} \\ &= \begin{pmatrix} \gamma & \text{Tr}(B) \\ \text{Tr}(B) & 1-\gamma \end{pmatrix}, \end{aligned} \quad (\text{S2})$$

where the second equality comes from the fact that, Pauli channels are trace preserving. It is easy to see that $\text{Tr}(B)$ is a real number, so comparing Eq. S1 and S2 at $\gamma=1/2$, we can see that $S_2=2\text{Tr}(B)$ and $S_1=S_3=0$. Thus we consider the effect of the quantum switch on the S_2 component of the control, note that to distinguish the operations on the control and target, we use $\sigma_0^c, \sigma_1^c, \sigma_2^c$ and σ_3^c for the control qubit and $\sigma_0, \sigma_1, \sigma_2$ and σ_3 for the target qubit,

$$\begin{aligned} S_2(\mathfrak{s}[\mathcal{N}_p, \mathcal{N}_q]) &= \text{Tr} \{ (\sigma_1^c \otimes \sigma_0) \cdot \mathfrak{s}[\mathcal{N}_p, \mathcal{N}_q] \} \\ &= \sum_{i,j} p_i q_j \text{Tr} \{ (\sigma_1^c \otimes \sigma_0) \cdot \mathfrak{s}[\sigma_i, \sigma_j] \} \\ &= \sum_{i,j} p_i q_j S_2(\mathfrak{s}[\sigma_i, \sigma_j]) \end{aligned} \quad (\text{S3})$$

The above equation shows that with knowledge of the control qubit for individual combinations of σ_i, σ_j we can get the S_2 of the switch with channels \mathcal{N}_p and \mathcal{N}_q .

From Eq. S3, we get $\tilde{\rho}_c$, and we can calculate the von Neumann entropy $H(\tilde{\rho}_c)$, which is necessary to obtain the Holevo capacity as shown in Eq. 9. The other quantity needed to evaluate 9 is the minimum entropy of the total output $H^{\min}(\mathfrak{s}[\mathcal{N}_p, \mathcal{N}_q])$. In order to calculate this, let us first write the action of the quantum switch, in terms of individual combinations of Pauli operations:

$$\begin{aligned} \mathfrak{s}[\mathcal{N}_p, \mathcal{N}_q](\rho_c \otimes \rho_t) &= \sum_{i,j} p_i q_j (\gamma |0\rangle\langle 0|_c \otimes \sigma_i \sigma_j \rho_t \sigma_i^\dagger \sigma_j^\dagger \\ &\quad + (1-\gamma) |1\rangle\langle 1|_c \otimes \sigma_j \sigma_i \rho_t \sigma_i^\dagger \sigma_j^\dagger \\ &\quad + \sqrt{\gamma(1-\gamma)} |0\rangle\langle 1|_c \otimes \sigma_i \sigma_j \rho_t \sigma_i^\dagger \sigma_j^\dagger \\ &\quad + \sqrt{\gamma(1-\gamma)} |1\rangle\langle 0|_c \otimes \sigma_j \sigma_i \rho_t \sigma_i^\dagger \sigma_j^\dagger) \\ &= \sum_{i,j} p_i q_j \mathfrak{s}[\sigma_i, \sigma_j](\rho_c \otimes \rho_t) \end{aligned} \quad (\text{S4})$$

From Eq. S4, we notice that from pairwise combinations of σ_i and σ_j operators we can find out the output $\mathfrak{s}[\mathcal{N}_p, \mathcal{N}_q](\rho_c \otimes \rho_t)$ and its minimum entropy $H^{\min}(\mathfrak{s}[\mathcal{N}_p, \mathcal{N}_q])$, given we use an optimised target state ρ_t . Note that, the operations in $\{\sigma_i\}$ either commute or anti-commute. We can construct $\mathfrak{s}[\sigma_i, \sigma_j](\rho_c \otimes \rho_t)$ by projecting the control qubit into the diagonal/antidiagonal basis which results to a product state. Denoting the anti-commutator by $\{\dots\}$ and the commutator by $[\dots]$, we have, with $\gamma=1/2$,

$$\mathfrak{s}[\sigma_i, \sigma_j](\rho_c \otimes \rho_t) = \begin{cases} |+\rangle\langle +|_c \otimes \{\sigma_i, \sigma_j\} \rho_t \{\sigma_i, \sigma_j\}^\dagger \\ \text{for } [\sigma_i, \sigma_j] = 0 \\ |-\rangle\langle -|_c \otimes [\sigma_i, \sigma_j] \rho_t [\sigma_i, \sigma_j]^\dagger \\ \text{for } \{\sigma_i, \sigma_j\} = 0 \end{cases}.$$

The value of the Stokes parameter $S_2(\mathfrak{s}[\sigma_i, \sigma_j])$, which is 1 (-1) for commuting (anti-commuting) operations in the ideal case, can be experimentally obtained by noting that $S_2(\mathfrak{s}[\sigma_i, \sigma_j]) = \text{Tr}[(\sigma_1^c \otimes \sigma_0) \mathfrak{s}[\sigma_i, \sigma_j](\rho_c \otimes \rho_t)]$, i.e., expectation value of the operator $\sigma_1^c \otimes \sigma_0$.

Experimental details

Our experimental setup is adapted from the quantum switch of Ref. [11], removing cylindrical lenses and using only inverting prisms, since only Pauli operations where necessary, Fig. S1. Our input light is diagonally-polarised ($|\rho_c\rangle = (|0\rangle + |1\rangle)/\sqrt{2} = D$), and is in the first-order spatial mode ($|\rho_t\rangle = |1\rangle = \text{HG}_{10}$).

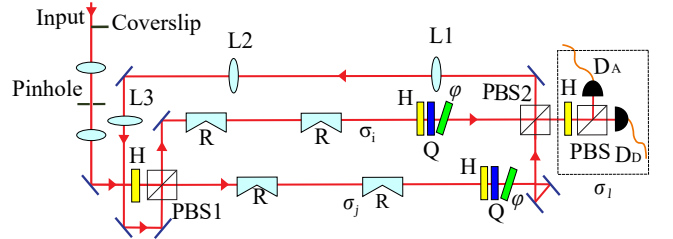


FIG. S1. Schematic of quantum switch. R is the rotating prism S5, H and Q are the half and quarter waveplates respectively and φ are the phase plates. The control qubit is the polarisation, $|\psi_c\rangle = D$. The polarisation of the light controls order of Pauli operations $\{\sigma_i\}$ acting on the photonic spatial mode $|\psi_t\rangle = \text{HG}_{10}$, for horizontal polarisation H, the order is $\sigma_i \circ \sigma_j$, for the vertical polarisation V the order is $\sigma_j \circ \sigma_i$. The polarisation D ensures superposition of the orders. X is a polarisation measurement, determining the Stokes parameter of the measured photon in the diagonal/anti-diagonal basis. Lenses L1 to L3 form a telescope for mode-matching.

We realise the unitary operations $\{\sigma_i\}$ using a pair of rotating prisms [20] as shown in Fig. S1. A mechanical rotation of the inverting prism results in a rotation of the incoming spatial mode of the photon, the outputs of the combined operation $\{\sigma_i \circ \sigma_j\}$ are shown in Fig. 2.

Unitary	φ	θ_1	θ_2
σ_0	0	$\frac{\pi}{2}$	$\frac{\pi}{2}$
σ_1	0	$\frac{\pi}{4}$	$\frac{\pi}{4}$
σ_2	$\frac{\pi}{2}$	$\frac{\pi}{2}$	$\frac{\pi}{4}$
σ_3	0	$\frac{\pi}{2}$	$\frac{\pi}{4}$

TABLE S1. Phases and angles for the unitary operations realised in our experiment, given by Eq. S6.

To implement σ_i, σ_j , we use up to two rotating prisms [11] in each arm. Each prism is oriented at a physical angle θ , which reflects and rotates an incoming beam by 2θ . The action of the rotating prism on our target qubit subspace is represented by the following unitary operation:

$$R(\theta) = \begin{pmatrix} -\cos 2\theta & \sin 2\theta \\ \sin 2\theta & \cos 2\theta \end{pmatrix}. \quad (\text{S5})$$

We impart the global phase φ by a tilted phase plate. We write the transformation performed by the pair of prisms and the phase plate as:

$$U(\varphi, \theta_1, \theta_2) = e^{i\varphi} R(\theta_2) R(\theta_1). \quad (\text{S6})$$

We place the phase plate only when we are doing σ_2 operation. For operations, σ_1 and σ_3 we need only one rotating prism, and for σ_0 and σ_2 we need both prisms. We achieve this by moving the second rotating prism via a translation stage. Table S1 are the angles and phases used to implement the Pauli operations. Since this rotation also changes the polarisation of the field—the control qubit—which is not desired, this rotation is cancelled after the two rotating prisms by the actions of the half- (H), and quarter- (Q) waveplates and the phase plate (ϕ), see Figure S1.

We emphasise that in our architecture, the sender cannot access the individual channels—channels \mathcal{N}_p or \mathcal{N}_q —without using the other one. That is, when we consider combinations of channels where one of the channels is unitary, this unitary channel cannot be accessed without also going through the noisy channel. This is certainly not a unique realisation of indefinite causal order. For example, one can use a Sagnac interferometer to achieve the same indefinite causal order as in Ref 12 of the main paper.

Effects of experimental imperfections

We note, the Pauli operations we are implementing by the rotating prisms, can be non-ideal due to uncertainty of the angles. This can affect the experiment in two ways. First, it leads to non-zero S_1 and S_3 Stokes parameters in the output control qubit and second, these nonzero terms contribute to $H^{\min}(\mathfrak{s}[\mathcal{N}_p, \mathcal{N}_q])$. To account for this issue, we note that the uncertainty associated with our rotation mounts is $\pm 1^\circ$. We numerically introduce random uniformly distributed error of $\pm 1^\circ$ to the angles of the rotating prisms. We repeat the simulation for 500 iterations and measure the capacity in each run. We confirm that the contribution of the random errors are well

within the range of our experimental visibilities, which is reflected in the orange shades of the graphs in the Fig. 3, 4, S3, and S5.

More general combinations of depolarising and dephasing channels

In the main section we have introduced a combination of depolarising channel of strength q and a dephasing channel of strength p as shown in Eq.11. We have shown the special case for $p=1$ where it is possible to achieve unit Holevo capacity. In this section we show more general situations where $p \leq 1$. In Fig. S2, the black lines show the cases for either $p=0.5$, $p=0.8$, or $p=1$ combined with a depolarising channel of strength q in an indefinite order. The blue line shows the capacity when these channels are in definite order, which regardless of the value of p monotonically decreases to zero when $q=1$. In contrast, with indefinite order arrangements the predicted Holevo capacities are 0.31 bits, 0.61 bits and 1 bit for $p=0.5$, $p=0.8$ and $p=1$ respectively. In Fig. S3 we plot the logarithm of Holevo capacities as a function of both depolarising channel strength q for 2 different strengths of the dephasing channel, $p=0.5$, and $p=0.8$. The black curves on the graphs show the predicted Holevo capacity for the indefinite order, the orange shade is the uncertainty due to the fringe visibility and the red dots are experimental data points. In the case of $p=0$, the dephasing channel behaves as an identity channel and the input state ρ_t is equally scrambled in both definite and indefinite order cases, thus resulting no overall advantage. However, in other cases there is non-zero information-theoretic advantage. At a full depolarising strength of $q=1$: in the case of $p=0.5$, the predicted $\chi_i=0.31$ bits, whereas we experimentally show 0.179 ± 0.006 bits; at $p=0.8$, the predicted $\chi_i=0.61$ bits, we experimentally show 0.42 ± 0.01 bits.

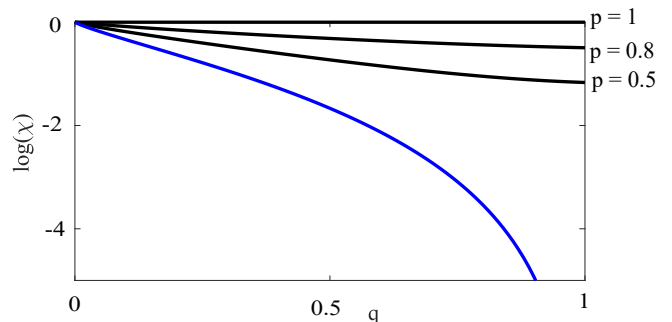


FIG. S2. Predicted logarithm of Holevo capacity χ for the channels in Eq. 11 vs. depolarisation noise strength, q . The solid black lines are for indefinite order in the cases of $p=0.5$, $p=0.8$, and $p=1$. The solid blue line are for definite order, regardless of the value of p , the combination of the dephasing and depolarising channels scramble the information equally. At the full depolarisation strength, $q=1$, $\chi_d=0$ whereas χ_i are 0.31 bits, 0.61 bits, and 1 bit in case of $p=0.5$, $p=0.8$, and $p=1$ respectively.

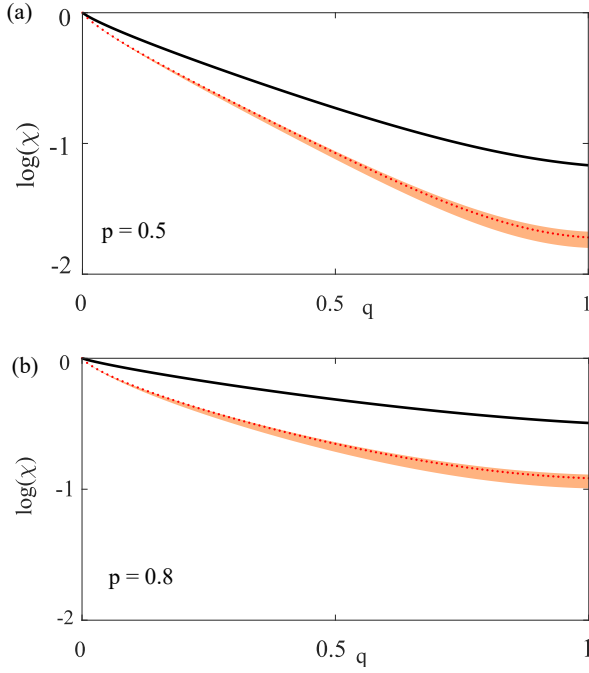


FIG. S3. Logarithm of Holevo capacity χ , where one channel is a depolarising channel of varying strength q , and the other one is a dephasing channel of strength p . The solid black lines are the theoretical predictions for Holevo capacity for indefinite causal order. The orange shades show the uncertainty due to non-ideal visibility in our experiment. The red dots are the experimentally measured data points. (a) shows the case when $p=0.5$. In this case the ideal value is $\chi_i=0.31$ bits whereas we experimentally measure 0.179 ± 0.006 bits. (b) is the case when $p=0.8$. Here, the χ_i is 0.61 bits and we measure 0.42 ± 0.01 bits.

Bit flip and bit-phase-flip channels

Consider two noisy channels, a bit-flip and a bit-phase-flip channel with strength p given, correspondingly, by

$$\begin{aligned} N_p^1(\rho_t) &= (1-p)\rho_t + p\sigma_1\rho_t\sigma_1, \\ N_p^2(\rho_t) &= (1-p)\rho_t + p\sigma_2\rho_t\sigma_2. \end{aligned} \quad (\text{S7})$$

Then,

$$\begin{aligned} \epsilon_+(\rho_t) &= (1-p)^2\rho_t + p(1-p)(\sigma_1\rho_t\sigma_1 + \sigma_2\rho_t\sigma_2) \\ \epsilon_-(\rho_t) &= p^2\sigma_3\rho_t\sigma_3. \end{aligned} \quad (\text{S8})$$

It should be highlighted that the outcome corresponding to the $|-\rangle\langle -|$, namely the $\epsilon_-(\rho_t)/p^2$ channel, is actually a purely unitary channel, capable of achieving perfect transmission despite both channels being noisy (as was also pointed out recently in Ref.[7]). However, here we are interested in the Holevo capacity resulting from considering both possible outcomes weighted by their corresponding probabilities, rather than the post-selected $\epsilon_-(\rho_t)$. We solve the corresponding minimization problem to compute the Holevo capacity. Fig.

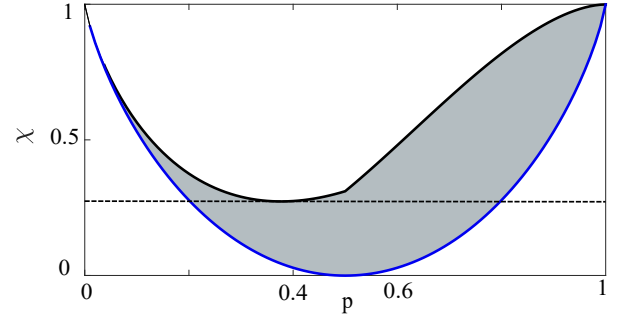


FIG. S4. Predicted Holevo capacity χ for the channels in Eq. S7 versus noise parameter, p . The solid black line is the Holevo capacity of depolarising channels in indefinite order and the solid blue line is for the case of definite order. We observe a knee at $p=0.5$, this is because the optimum state for $p \leq 0.5$ are the eigenvectors of the operator σ_1 and σ_2 . On the other hand, for $p \geq 0.5$ the optimum state is the eigenvector of σ_3 . At $p=0.5$, the definite-ordered channel becomes completely depolarising, making $\chi_d = 0$, whereas at this point $\chi_i = 0.31$ bits. In the region of $p \geq 0.5$, the maximum difference between the two cases is 0.55 bits, occurring when $p=0.75$. The black horizontal dashed line denotes the minimum capacity of the indefinite-ordered case, 0.27 bits when $p=0.37$.

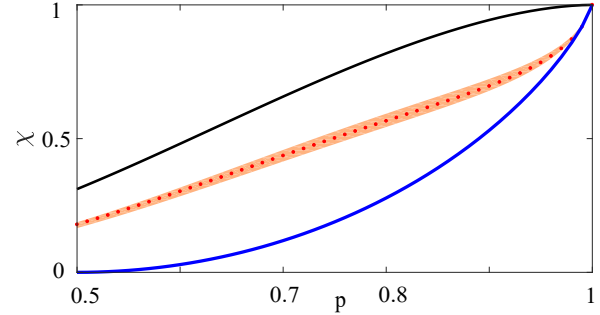


FIG. S5. Experimental Holevo capacity χ for $p \geq 0.5$ region, where one channel is a bit-flip channel and the other one is a dephasing channel with varying strength p as in the Eq. S7. The solid black line is the theoretical predictions for Holevo capacity for indefinite causal order. The blue line is the theoretical prediction for Holevo capacity for definite causal order. The red dots are the experimental data points and the orange shade is the expected range due to non-ideal visibility. At $p=0.5$, the experimentally measured Holevo capacity is 0.179 ± 0.006 bits, whereas $\chi_d=0$.

S4 plots the Holevo capacity χ against different noise parameters p for both the cases of noisy channels in a definite order, and in an indefinite order. The black curve is the Holevo capacity for indefinite order, while the blue curve is for definite order. As shown by the difference of these two curves, indefinite order provides an advantage over the definite-order case. Indefinite order allows transmission of 0.27 bits or more over the whole range of p values. The minimum capacity of 0.27 bits which occurs at $p=0.37$, is higher than the capacity of the definite-order case from $p=0.2$ to $p=0.8$, 60% of the range of p . The maximum advantage $\max[(\chi_i - \chi_d)] = 0.55$ bits occurs at $p=0.75$, where the Holevo capacity for the quantum switch

and definite order cases are 0.75 bits and 0.19 bits, respectively. We can see there is a knee in the χ_i at noise parameter $p=0.5$. This is because when $p \leq 0.5$, the eigenvectors of σ_1 or σ_2 achieve the minimum entropy $H^{\min}(\mathfrak{s}[\mathcal{N}_p^1, \mathcal{N}_p^2])$, while for $p \geq 0.5$, the corresponding optimum state turns out to be the eigenvectors of σ_3 . When $p=0.5$, where the classical order results in full depolarization, the capacity resulting from indefinite order is $\chi_i \approx 0.31$ bits. In this case, any of the eigenstates of the Pauli operator achieves the maximum capacity thus increasing the domain over which we can optimally encode the input.

Holevo capacity from path superposition

Although the advantage in communication is not unique to superposition of order, there is strong reason to believe that the perfect transmission discussed above is not possible via a superposition of paths, where we place two noisy channels in two arms of an interferometer [16]. The optimised Holevo capacity that we obtain for a fully depolarising channel and a unitary channel in path superposition is 0.75 bits. Moreover, we prove that reaching a value of 1 bit is impossible:

In our communication task, we consider the target system, the control system and two Pauli channels to transfer the target qubit. The control enables the target to go through a superposition of paths. In our experiment, $|\psi_c\rangle$ is set to be $|+\rangle$, the target state is optimized to achieve the maximum communication capacity, and a generalized measurement on the control system is applied after noisy channels.

We consider our Pauli channels to be the depolarising channel, \mathcal{N} , as shown in Eq. 10, and σ_3 . Following [16], after tracing out the environment, the output control and target state takes the following form:

$$\rho_{tot}^{(ct)} = \frac{1}{2} \left(|0\rangle\langle 0|^c \otimes \mathcal{N}(\rho_t) + |1\rangle\langle 1|^c \otimes \sigma_3 \rho_t \sigma_3 + |0\rangle\langle 1|^c \otimes T_0 \rho_t \sigma_3 + |1\rangle\langle 0|^c \otimes \sigma_3 \rho_t T_0^\dagger \right) \quad (\text{S9})$$

where $T_0 = \sum_i e_i K_i$, K_i are arbitrary choices for Kraus operators for the depolarising channel with the constraint $\sum_i |e_i|^2 = 1$. Exploiting the unitary freedom in the operator-sum representation (see for example Ref. [21]), one has that

$$\sin^2 2\alpha \left[(r_2^{(in)} f_{0,I} - r_3^{(in)} f_{1,R} + r_1^{(in)} f_{3,R} + f_{2,I})^2 + (r_1^{(in)} f_{0,I} + r_3^{(in)} f_{2,R} + f_{1,I} - r_2^{(in)} f_{3,R})^2 + (f_{0,R} + r_1^{(in)} f_{1,R} + r_2^{(in)} f_{2,R} + r_3^{(in)} f_{3,R})^2 \right] + \cos 4\alpha = 2 \quad (\text{S16})$$

Next we proceed to show that, Eq. S16 cannot hold under conditions S14 and $\sum_i |f_i|^2 = \sum_i \sum_{k \in \{R,I\}} f_{i,k}^2 = 1$. Note that

$e_i K_i = e_i \sum_j U_{i,j} \frac{\sigma_j}{2}$, with $U_{i,j}$ the entries of a unitary matrix, and thus $T_0 = \sum_j (\sum_i e_i U_{i,j}) \frac{\sigma_j}{2} \equiv \sum_j f_j \sigma_j / 2$, with $\sum_j |f_j|^2 = 1$. Now if we measure the control qubit in the $\{M_+, M_-\}$ basis,

$$\begin{aligned} M_+ &= \cos \alpha |0\rangle + \sin \alpha |1\rangle, \\ M_- &= -\sin \alpha |0\rangle + \cos \alpha |1\rangle, \end{aligned} \quad (\text{S10})$$

the two possible output states, with corresponding probabilities p_+ and p_- , are given by

$$\begin{aligned} p_+ \rho_+^t &= \frac{1}{4} \left[\cos^2 \alpha \frac{\sigma_0}{2} + \sin^2 \alpha \sigma_3 \rho_t \sigma_3 + \frac{\cos \alpha \sin \alpha}{2} \sum_i (f_i \sigma_i \rho_t \sigma_3 + f_i^* \sigma_3 \rho_t \sigma_i) \right], \\ p_- \rho_-^t &= \frac{1}{4} \left[\sin^2 \alpha \frac{\sigma_0}{2} + \cos^2 \alpha \sigma_3 \rho_t \sigma_3 - \frac{\cos \alpha \sin \alpha}{2} \sum_i (f_i \sigma_i \rho_t \sigma_3 + f_i^* \sigma_3 \rho_t \sigma_i) \right]. \end{aligned} \quad (\text{S11})$$

where f_i^* is the complex conjugate of f_i .

Now, achieving a unit Holevo capacity implies that both the input and output state must be pure. In the Bloch representation, this implies that

$$\sum_i |r_i^{(+)}|^2 = 1, \quad (\text{S12})$$

$$\sum_i |r_i^{(-)}|^2 = 1, \quad (\text{S13})$$

$$\sum_i |r_i^{(in)}|^2 = 1 \quad (\text{S14})$$

where $\{r_i^{(+)}\}$, $\{r_i^{(-)}\}$ and $\{r_i^{(in)}\}$ are the Bloch vector components of the projected states ρ_+^t , ρ_-^t and the input target state, ρ_t respectively. We proceed by writing f_i into its real and imaginary parts, i.e., $f_j = f_{j,R} + i f_{j,I}$. Then, from $\sum |r_i^{(+)}|^2 = \sum |r_i^{(-)}|^2$ we find that

$$\sin 2\alpha (r_3^{(in)} f_{0,R} + f_{3,R} + r_1^{(in)} f_{2,I} - r_2^{(in)} f_{1,I}) + \cos 2\alpha = 0 \quad (\text{S15})$$

which can be replaced into $\sum |r_i^{(+)}|^2 + \sum |r_i^{(-)}|^2 = 2$ to obtain

for this purpose, it is sufficient to prove that

$$\begin{aligned} F(r, f) &= (r_2^{(in)} f_{0,I} - r_3^{(in)} f_{1,R} + r_1^{(in)} f_{3,R} + f_{2,I})^2 \\ &+ (r_1^{(in)} f_{0,I} + r_3^{(in)} f_{2,R} + f_{1,I} - r_2^{(in)} f_{3,R})^2 \\ &+ (f_{0,R} + r_1^{(in)} f_{1,R} + r_2^{(in)} f_{2,R} + r_3^{(in)} f_{3,R})^2 < 3. \end{aligned} \quad (\text{S17})$$

Exploiting the relation that $2xy \leq x^2 + y^2$ for any real x and y , Eq. S14, and that for that for $|r_i| \leq 1$ one has that $r_i \leq |r_i|$ and $|r_i|^2 \leq |r_1|$, we have

$$\begin{aligned}
F(r, f) &\leq (1 + r_1^{(in)} + r_2^{(in)} + |r_3^{(in)}|^2) f_{0,I}^2 + (1 + r_1^{(in)} + r_2^{(in)} + r_3^{(in)}) (f_{0,R}^2 + f_{1,I}^2 + f_{2,I}^2 + f_{3,R}^2) \\
&\quad + (1 + r_1^{(in)} + |r_2^{(in)}|^2 + r_3^{(in)}) f_{1,R}^2 + (1 + |r_1^{(in)}|^2 + r_2^{(in)} + r_3^{(in)}) f_{2,R}^2 \\
&\leq (1 + |r_1^{(in)}| + |r_2^{(in)}| + |r_3^{(in)}|) \sum_i |f_i|^2 \\
&\leq 1 + \sqrt{3 \sum_i |r_i^{(in)}|^2} \\
&\leq 1 + \sqrt{3} < 3,
\end{aligned} \tag{S18}$$

as desired. This supports the idea that \mathcal{N} and a unitary channel

in a superposition of paths cannot lead to a pure output and thus cannot achieve unit Holevo capacity.